Journal of the Civil Engineering Forum, January 2024, 10(1):59-72
DOI 10.22146/jcef.9929
Available Online at https://journal.ugm.ac.id/v3/jcef/issue/archive

Analysis of Gongseng Dam Break-Induced Flood in East Java, Indonesia Through 2D Iber Software

Sa'iyd Husayn Ahmadi[1], Bambang Triatmodjo[1,2], Benazir[1,*]
[1]Department of Civil and Environmental Engineering, Universitas Gadjah Mada, Yogyakarta, INDONESIA
Jalan Grafika No 2 Yogyakarta
[2]Center for Environmental Studies, Gadjah Mada University, Special Region of Yogyakarta 55281, INDONESIA
*Corresponding author: benazir@ugm.ac.id

SUBMITTED 19 September 2023 **REVISED** 07 November 2023 **ACCEPTED** 14 November 2023

ABSTRACT The dam is a crucial river-crossing structure that ensures a sustainable water supply and offers numerous benefits. However, the potential hazard of dam failure is an imminent threat that could materialize unexpectedly. To comprehend the potential impact of dam break flood and identify vulnerable areas, it is essential to conduct rigorous analysis and simulate various dam failure scenarios. This comprehensive assessment is invaluable for informed land use planning and the development of effective emergency response plans. Therefore, this study aimed to analyze flood inundation resulting from the hypothetical failure of Gongseng dam, using Iber model. The modeling approach relied on a two-dimensional finite volume shallow water model, guided by specialized software. The scenarios for Gongseng dam break showed inundation areas of 12.57 km^2 and 7.55 km^2 for overtopping and piping failure, respectively. Overtopping failure resulted in the highest discharge, with Von Thun method causing severe damage due to wide break dimensions, and eventually leading to catastrophic consequences. However, this study showed that Froehlich method provided the most rational prediction for break parameters. In contrast to the other methods focusing solely on water height behind dam, Froehlich equation considered both the volume and height at the time of failure. Implementing dam break analysis held the potential to benefit downstream communities by providing inundation maps, thereby aiding in the mitigation of flood risks. Particularly, in situations with limited data and resources, as shown in this study, the cost-effective modeling method proposed could be an attractive option for simulating extreme flood induced by dam break.

KEYWORDS Dam Break Analysis; Break Parameters; Flood Inundation; Flood Routing; Iber

1 INTRODUCTION

The maintenance of sustainable water resources is challenged by factors such as population growth, restricted water availability, and increasing droughts. Therefore, strategic management of water resources is essential to meet diverse demands, including irrigation, water supply, groundwater recharge, and hydroelectricity. Acknowledging the significance of rivers in business activities and human existence, effective management should consider fundamental needs and pursue sustainable economic growth (Guo et al., 2022). Achieving an appropriate allocation of demands for river flows is inherently challenging, requiring effective regulation considering socio-economic and ecological sustainability aspects. Therefore, strategic development is essential to ensure rational and efficient allocation of water resources in a river basin. Dam is significant infrastructure for securing a water supply by controlling stream flow and establishing reservoir (Khosravi et al., 2016).

Situated in Kedungsari Village, Temayang District, Bojonegoro Regency, East Java Province, Gongseng Dam plays a crucial role in impounding Soko River, resulting in a water volume of 22.47 million cubic m. Bengawan Solo River Basin Agency 2021 Database of Water Resources Information shows various benefits of Gongseng Reservoir, including supplementary irrigation covering 6191 ha with a planting intensity of 250%, a water supply of 300 l s^{-1}, groundwater recharge, and a 20% reduction in peak flood discharge (133.27 m^3 s^{-1}). Despite these advantages, the pending threat of dam failure is ever-present. A potential collapse could lead to a large-volume flood, posing a significant threat to life and property down-

stream. Emergency response plans should consider factors such as property damage, loss of life, environmental impact, and landscape disruption (Bharath et al., 2021). Categorized as a medium-sized dam by da Hora et al. (2018), Gongseng falls in the range of 15 to 30 m in height and reservoir volumes between 1 to 50 million m^3. In terms of technical risk, dam is classified as low, showing a minimal possibility of structural failure due to engineering errors, operational failure, maintenance negligence, damage, or monitoring lapses. The potential for governance-induced damage is extremely low. However, concerning potential damage capacity, Gongseng Dam falls into the high-risk category.

Mandatory monitoring activities capable of detecting early signs of dam failure need to be conducted. These monitoring activities should be seamlessly integrated with dam operation and maintenance procedures. Although monitoring in isolation is considered insufficient, the implementation of mitigation strategies should be based on a well-defined emergency response plan. Oliveira et al. (2022) showed that the graphical methods for calculating non-permanent flow resulting from dam break originated with Craya and Re in 1946. evolving into a framework for dam management authorities to implement emergency procedures.

Break mechanisms can be triggered by various factors, but for the sake of simplicity, this study assumes only two failure scenarios. Determining break parameters necessitates meeting absolute conditions, such as ensuring the bottom elevation is not lower than the foundations and the final break width is less than the abutment (Wahl, 2004). The two-dimensional model is most widely recognized for simulating flood and inundation due to dam break (Kao and Chang, 2012; Álvarez et al., 2017). The depth-averaged shallow water equations, also known as two-dimensional St. Venant Equations (2D-SWE), are solved using numerical methods. These equations consider a

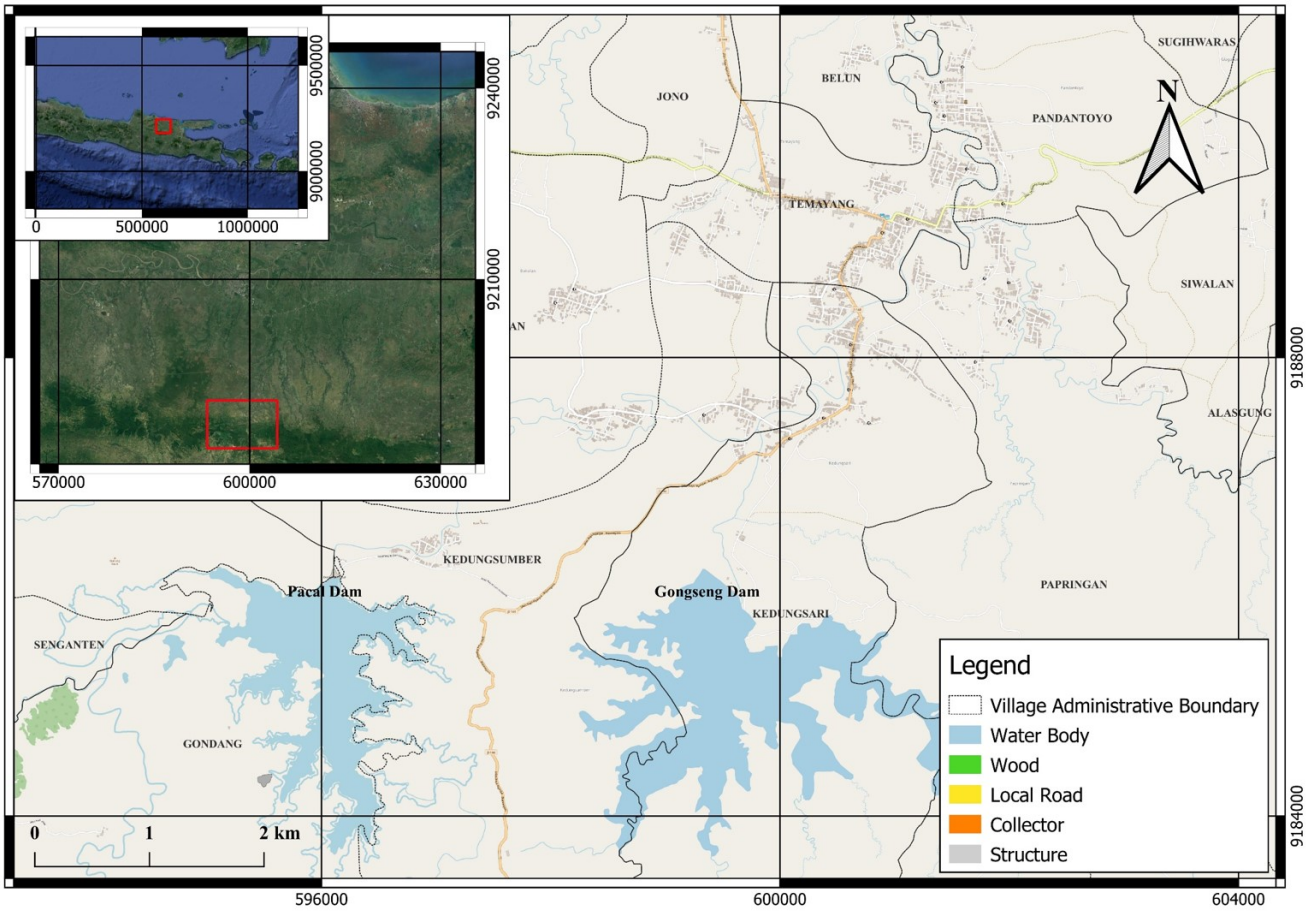

Figure 1 Study area at Gongseng dam

hydrostatic pressure distribution and a relatively uniform depth velocity distribution (Wu, 2004). The primary focus of this analysis is the examination of the outflow hydrograph arising from dam infractions with varying break parameters. This study aims to predict essential characteristics of the ensuing flood waves at Gongseng Dam, including peak flood discharge, timing of the occurrence, and the routing of the hydrograph for different downstream sections of the river course. Additionally, the generation of inundation maps for various dam failure scenarios is included in the investigation.

2 STUDY METHODOLOGY

This study simulated the potential failure of Gongseng Dam in Bojonegoro. Mathematical models were adopted to simulate scenarios and identify inundation area downstream. The study methodology was established through a review of appropriate literature, and data organization was conducted based on the availability of the sources and study needs.

$$\frac{\partial h}{\partial t} + \frac{\partial hU_x}{\partial x} + \frac{\partial hU_y}{\partial y} = M_s \qquad (1)$$

Flood routing was conducted in this study, depicting the study area in Figure 1 which consisted of six villages, namely Kedungsari, Kedungsumber, Papringan, Temayang, Pandantoyo, and Belun. The optimal time for running flood models due to dam break was determined when inundation had not significantly evolved (Bo et al., 2015; Khosravi et al., 2016; Álvarez et al., 2017; Bharath et al., 2021). Google Earth imagery estimated the distance between dam area and rural area at approximately 1.22 km, covering a total study area of 35.22 km^2.

Incorporating two primary steps in the study, the first included routing breach flood hydrographs downstream, while the second focused on generating floodplain maps for various dam failure modes. The dam break analysis used the Iber hydraulic model, incorporating a previously developed finite volume scheme for solving the two-dimensional shallow water equations in hydrological applications. Iber proved effective in simulating 2D dam break wave, impacting an obstacle downstream of dam. This induced the generation of a hydraulic jump upstream of the obstacle and a weak zone downstream (Cea et al., 2010; Cea and Bladé, 2015). Iber adopted flood routing methods proposed by depth-averaged shallow water equations (2D-SWE) for unsteady flow (Bladé et al., 2014; Bladé, Cea, Corestein, Escolano, Puertas, Vázquez-Cendón, Dolz and Coll, 2014; Cea Gómez et al., 2019). The depth-integrated continuity and conservation of momentum were as in Equation 2 and Equation 3.

Where h is the flow depth, t is time, x and y are the horizontal cartesian coordinates, U_x and U_y are the depth-averaged flow velocities in the x and y directions, and Z_s is the water surface elevation. Other factors included g for acceleration due to gravity, ρ for the density of the flow, ω for the Earth rotation angular velocity, λ for the latitude of the studied point, $_s$ for free surface friction due to wind-induced friction, $_b$ for bed friction, and $_x x^e$, $_x y^e$, as well as $_y y^e$ for effective horizontal tangential stresses. Additionally, M_s, M_x, and M_y served as the terms for mass source/drain and momentum, respectively, used to model precipitation, infiltration, and drainage.

The data processing commenced with the adjustment of raw data to make it suitable for computation in Iber software. Boundary conditions were a crucial input that significantly influenced the downstream water depth. The essential data for this study included hydrological information, comprising probable maximum precipitation (PMP) and 2-year return period precipitation, used as input for the synthetic unit hydrograph. According to Bengawan Solo River Basin Agency, the selected extreme rainfall event was

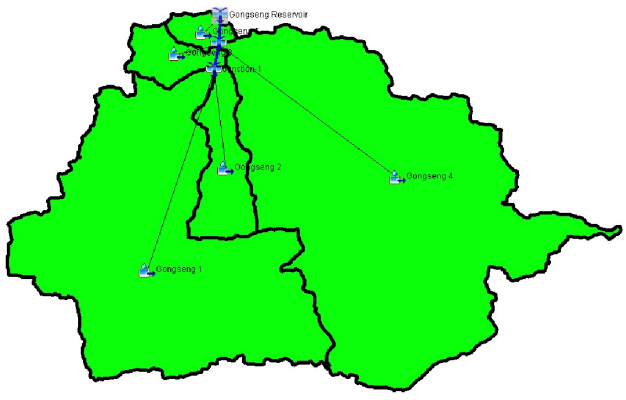

Figure 2 Basin models of Gongseng dam

$$\frac{\partial hU_x}{\partial t} + \frac{\partial hU_x^2}{\partial x} + \frac{\partial hU_xU_y}{\partial y} = -gh\frac{\partial hZ_s}{\partial x} + \frac{\tau_{s,x}}{\rho} - \frac{\tau_{b,x}}{\rho} - \frac{g}{\rho}\frac{h^2}{2}\frac{\partial \rho}{\partial x} + 2\sin\lambda U_y + \frac{\partial h\tau^e_{xx}}{\partial x} + \frac{\partial h\tau^e_{xy}}{\partial y} + M_x \quad (2)$$

$$\frac{\partial hU_y}{\partial t} + \frac{\partial hU_xU_y}{\partial x} + \frac{\partial hU_y^2}{\partial y} = -gh\frac{\partial hZ_s}{\partial y} + \frac{\tau_{s,y}}{\rho} - \frac{\tau_{b,y}}{\rho} - \frac{g}{\rho}\frac{h^2}{2}\frac{\partial \rho}{\partial y} + 2\sin\lambda U_x + \frac{\partial h\tau^e_{xy}}{\partial x} + \frac{\partial h\tau^e_{yy}}{\partial y} + M_y \quad (3)$$

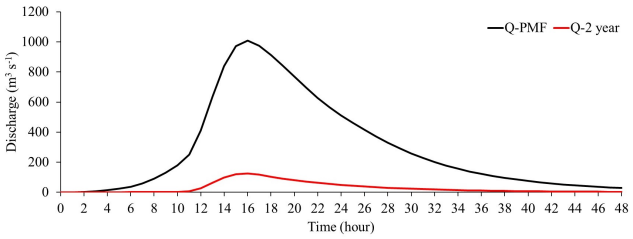

Figure 3 Flood hydrographs for PMF and 2-year return period

forecasted rain using Global Precipitation Measurement (GPM). The Snyder unit hydrograph was selected to simulate rainfall-runoff transformation, and the Green-Ampt method was applied for loss calculations. The boundary conditions, processed using HEC-HMS software, were shown in Figure 2, depicting flood routing scenarios in the hydrological model.

Probable maximum flood (PMF) and 2-year return period discharge (Q_2) served as the inlet boundary conditions upstream of Gongseng Reservoir. Flood hydrographs were generated probabilistically, therefore, both hydrographs were selected, as shown in Figure 3.

The hydrological analysis of Gongseng dam simulation indicated a peak flow of 1009 m^3 s^{-1} during PMF and 125.8 m^3 s^{-1} in 2-year return period. Gongseng Watershed was divided into five subwatersheds, with a total area of 51.21 km^2. The land use distribution map showed a dominance of woods and dryland agriculture in Gongseng subwatershed, with Pellic Vertisols and Lithosols as the predominant soil types (Balai Besar Wilayah Sungai Bengawan Solo, 2021).

Iber was capable of simulating dam failure along with its hydrological processes and could be installed as a plug-in. The intended hydrological model included processes related to loss due to infiltration, particularly in dry soil conditions. The loss method used in this study was the soil conservation service (SCS-CN), a simple method in-

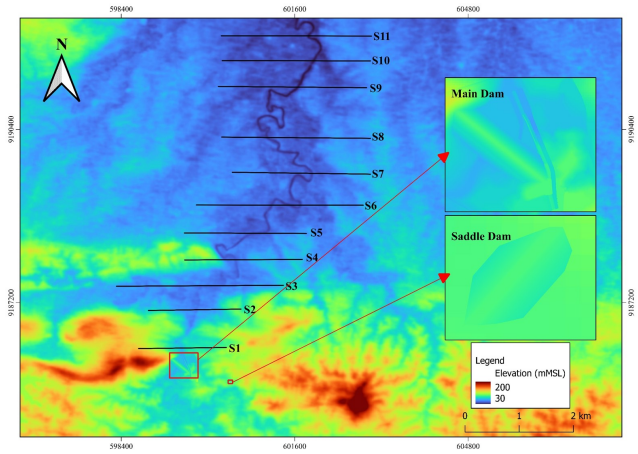

Figure 4 Subset of DEMNAS used for dam break simulation and cross-section of Soko-Pacal River

cluding specifying curve number (CN) values for each area and adjusting the initial abstraction coefficient values. CN values from Al-Weshah et al. (1993) were used in the simulation, assuming that the soil conditions were previously dry in flood area.

The turbulence model used an eddy viscosity technique based on the Boussinesq hypothesis. Iber provided a turbulence module to calculate the pressure, known as Reynolds stresses (Cea et al., 2007). These turbulent stresses were integrated with viscous strain and lateral dispersion terms, collectively termed effective pressure. The horizontal effective stresses appeared in the hydrodynamic equations of Iber. Downstream dam break modeling was analogous to open-channel flow models, and the shallow waters mixing length model, widely used for determining the turbulent viscosity ($_t$), was adopted (Jia and Wang, 1999). The advantage of this model lies in its simplicity in algebraic expression while remaining physically acceptable, considering bed friction and horizontal velocity gradient for resulting turbulence flow.

The geometry model was established using Quantum-GIS version 3.28.4, serving as the

Table 1. Predictions of average break width and failure time

Investigator	Overtopping		Piping	
	Average Break Width (m)	Failure time (min.)	Average Break Width (m)	Failure time (min.)
Froehlich (Fr)	116	89	68	84
Von Thun and Gillete (VTG)	115	44	102	38
Bureau of Reclamation (USBR)	72	48	57	38

foundation for the computation mesh. Elevation values from the National Digital Elevation Model (DEMNAS) were used as references in constructing the geometry model, correlating with topographic conditions illustrated in Figure 4. The processing of Digital Elevation Model (DEM) included using supporting tools, namely AutoCAD 2024 Student version and Ms. Excel 2016.

Break parameters were calculated using empirical methods developed by Froehlich (2008), Von Thun and Gillette (Bo et al., 2015), and USBR (U.S Department of The Interior Bureau of Reclamation, 1988). Froehlich equation incorporated both reservoir volume and the height of water behind dam, while Von Thun Gillette, and USBR equations solely considered the length. Break parameters obtained from these three empirical methods are presented in Table 1. Following the Guidelines for Dam Emergency Action Planning (Balai Bendungan, Direktorat Jenderal Sumber Daya Air, Kementrian Pekerjaan Umum dan Perumahan Rakyat, 2019), established at Makassar in 2019, three conditions were required for identifying flood inundation. Although this study only investigated two failure situations, the scenarios represented both extreme and common conditions. Dam failure due to piping (pip) was projected to occur during rainfall with 2-year return period resulting in normal flow (Q_2), with reservoir water level being normal. The second scenario included dam failure due to overtopping (ovt), corresponding to reservoir water level being similar to dam crest elevation, and PMF becoming an inlet boundary condition. Each of the scenarios was simulated using three different break formations.

3 RESULTS AND DISCUSSIONS

This study reported scenarios resulting from the overtopping and piping failure modes of Gongseng

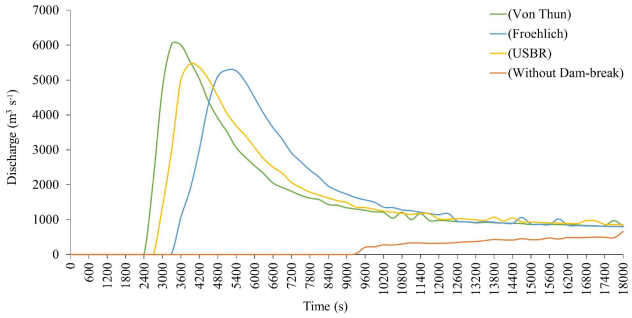

Figure 5 Downstream flood hydrographs for different empirical methods at +3.12 km from main dam

dam, along with presenting flood inundation map for the 7.8 km stretch downstream of reservoir. Additionally, the analysis provided valuable insights into the potential impacts and responses to dam failure in the specified conditions.

3.1 Flood Hydrographs

The hydrograph method comprised various parameters, with this sub-section specifically addressing the analysis of flood hydrographs. Figure 5 showed the distinct nature of flood hydrographs for each method. Von Thun method stood out by yielding the highest discharge with the shortest time to peak in comparison to others. This result correlated with the findings in Table 1, indicating that the VTG method exhibited the largest break volume and the shortest failure time.

This study delved into the investigation of flood wave propagation, aiming to determine arrival times and flow discharge at various cross-sections. Combining flood hydrographs at each cross-section into a unified chart provided insights into flood wave propagation. Flood hydrographs at various river sections downstream of dam, including 0.3 km, 1.1 km, 1.7 km, 2.3 km, 3 km, 3.6 km, 4.4 km, 5.5 km, 6.6 km, 7.3 km, and 7.8 km from dam for piping and overtopping failure were depicted in Figure 6 and Figure 7, respectively.

Figure 6 shows flood wave propagation from VTG method, known for causing the most severe damage. The attenuation of peak flow magnitude was observable as flood wave moved downstream. Based on VTG peak flow attenuation, section 1 reached 9070.33 m^3 s^{-1} with the shortest arrival time of 0.67 hours from the dam break inception. At section 2, peak flow started declining to

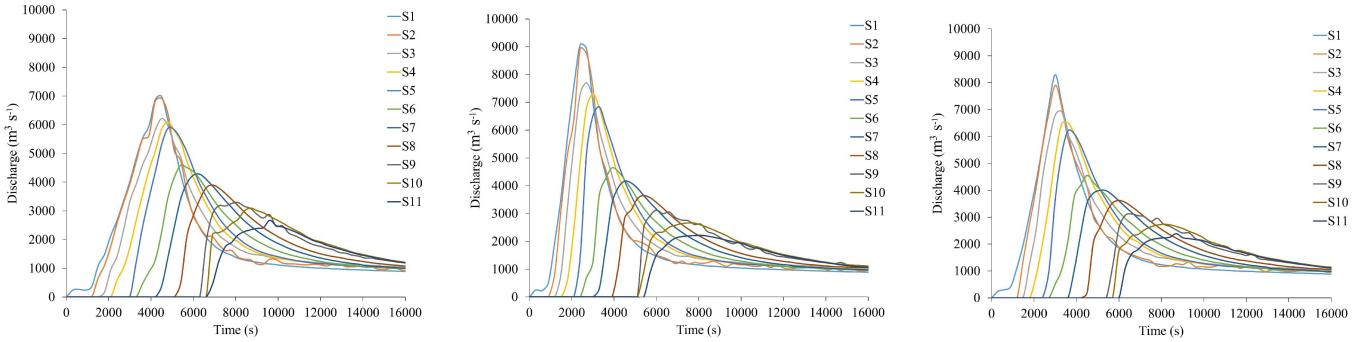

(a) Froehlich (b) Thun (c) USBR

Figure 6 Attenuation of flood hydrographs for overtopping as flood wave propagates downstream

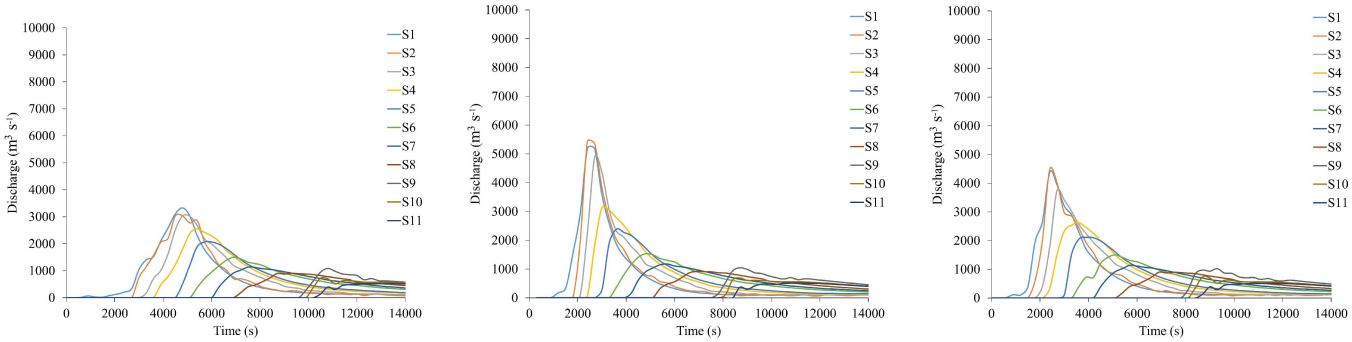

(a) Froehlich (b) Thun (c) USBR

Figure 7 Attenuation of flood hydrographs for piping as flood wave propagates downstream

8919.86 m^3 s^{-1} with a relatively similar arrival time to group 1. Flood hydrograph started decreasing at section 3, reaching a peak flow of around 7700.78 m^3 s^{-1}. Peak flow at section 4 stabilized at 7300.86 m^3 s^{-1}, and at section 5, it was 6840.21 m^3 s^{-1}. Flood hydrograph continued to descend until section 11, where attenuation percentages dropped to 309%, corresponding to 2216.3 m^3 s^{-1}. Peak flow attenuation percentages were relatively low in the higher reach (S1 to S5), while the lower side (S6 to S11) were particularly high.

The downstream discharge in piping scenario was lower than the flow in overtopping situation. This correlation was consistent with the initial conditions established for each scenario and break parameters for the methods. Figure 7 shows flood wave propagation for the three methods in the piping scenario. According to flood hydrograph results, VTG method produced the most severe peak discharge. Using this method in section 1, peak discharge value reached 5188.65 m^3 s^{-1}, with a longer arrival time of 0.58 h or 35 minutes compared to the overtopping failure of 5 minutes. Additionally, with an identical arrival time as section 1, peak flow started decreasing toward 5428.48 m^3 s^{-1} in category 2. Flood hydrograph started decreasing at section 3, reaching a peak flow of around 4878.16 m^3 s^{-1}. The maximum flood hydrograph at section 4 stabilized at 3125.9 m^3 s^{-1}, while the peak flow at section 5 showed 2387.01 m^3 s^{-1}. Flood hydrograph continued to decrease until it reached section 11, where peak hydrograph had dropped to 467%, corresponding to 511.25 m^3 s^{-1}. Flood hydrographs started flattening at section 11 and remained in the full capacity of the river banks, showing that the overtopping mode did not significantly affect inundation in rural area.

Time to peak was defined as the time for flood hydrograph to reach its discharge at a specific section and the arrival time of the wave. The time of arrival showed the time it takes for flood to reach a particular section. Figure 8 showed the time to peak and flood wave arrival time as a function of the distance from dam. According to Froehlich method, the time to peak of the hydrographs at sections 1, 2, and 3 in overtopping failure arrived at 1.25 h from the inception of the dam failure. The time to reach peak increased with the distance

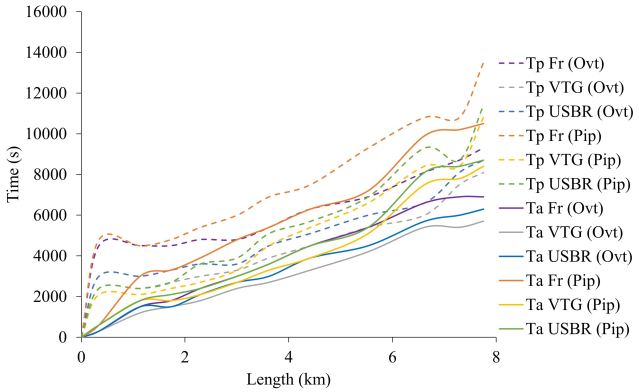

Figure 8 Time to peak (Tp) (dashed line) and flood wave arrival time (Ta) (solid line) versus distance from dam for empirical methods

from dam, consistent with the calculated break development time using empirical equations Comparing overtopping and piping failure, it was concluded that Von Thun overtopping formation had the shortest time to peak, as shown by an orange solid line. Considering that the time-to-peak values for overtopping were faster than for piping model, the fastest mode was considered the critical failure mode. Additionally, all results generated by dam failure simulation were sensitive to break parameters, prompting a comparison of the three approaches to determine the most reasonable parameters.

The chart pattern of time to peak and flood wave arrival time showed differences, primarily caused by the non-linear progression at each section, particularly downstream of dam. The arrival time showed a linear development between flood arrival time and the section distance, naturally increasing with distance resulting in a positive linear graph as confirmed by various methods. Similarly, with the time to peak, Von Thun method showed the fastest arrival time of 5 minutes for the first section. Flood wave continued downstream, arriving at the second section after 20 minutes with a distance of about 0.8 km, showing a 15-minute arrival time—a relatively short time for evacuating residents. In the last section, flood wave reached Belun Village after 1.58 hours, with the flow velocity ranging from 0.21 to 4.3 m s^{-1} between S1 and S11.

3.2 Flood Inundation Maps

Based on Figure 9, VTG method caused the most severe damage due to overtopping. Kedungsari Village experienced flood inundation reaching 4.51 m with average depth of 1.39 m, lasting for approximately 4.58 hours. About 500 m from Kedungsari, Kedungsumber faced a predicted depth of 4.83 m with average intensity of 1.95 m, inundated for 2.08 hours. Downstream of Kedungsari, Temayang Village, a crucial area known as the capital of Temayang District, estimated flood depth of 3.72 m with average of 1.49 m, lasting for 4.25 hours. Papringan Village near Temayang was impacted with an intensity of 2.96 m and average depth of 1.17 m, lasting for 4.08 hours. The downstream of Papringan was Pandantoyo Village, which experienced inundation up to 2.11 m with average depth of 0.78 m and lasted for 3.92 hours. In the final downstream section, Belun Village, the maximum flood depth was only 0.42 m with average intensity of 0.29 m, and inundation lasted for 0.75 hours.

Figure 10 showed that piping failure mode developed by VTG resulted in flood inundation in Kedungsari up to 2.54 m with average depth of 1.25 m, lasting for approximately 1 hour. A flood depth of 2.61 m with an average intensity of 1.54 m was faced by Kedungsumber, located approximately 500 m from Kedungsari, lasting for 0.75 hours. Temayang Village, a crucial area downflow of Kedungsari, had an estimated flood depth of 0.13 m and average of 0.12 m, lasting for only 0.33 hours. Perpignan also experienced flooding, with depth of 0.47 m, average intensity of 0.33 m, and inundation time of 0.75 hours. Towards the river's mouth of Papringan, inundation up to 0.19 m with an average depth of 0.14 m was experienced by Pandantoyo Village, lasting for 0.67 hours. However, Belun Village in the final downstream section was not affected by flood in piping failure mode.

3.3 Flood Velocity Maps

Figure 11 shows flood velocity based on the most severe damage due to overtopping failure mode. Flood velocity in Kedungsari Village exceeded 6.26 m s^{-1}, and the maximum velocity occurred rapidly with only 35 minutes after dam collapse. Kedungsumber Village had estimated flow velocity of 1.92 m s^{-1} with average speed of 0.84 m s^{-1}. Further along the river of Kedungsari, in Temayang Village, the estimated flood momentum was 1.26 m s^{-1} with average velocity of 0.2 m s^{-1}. A velocity

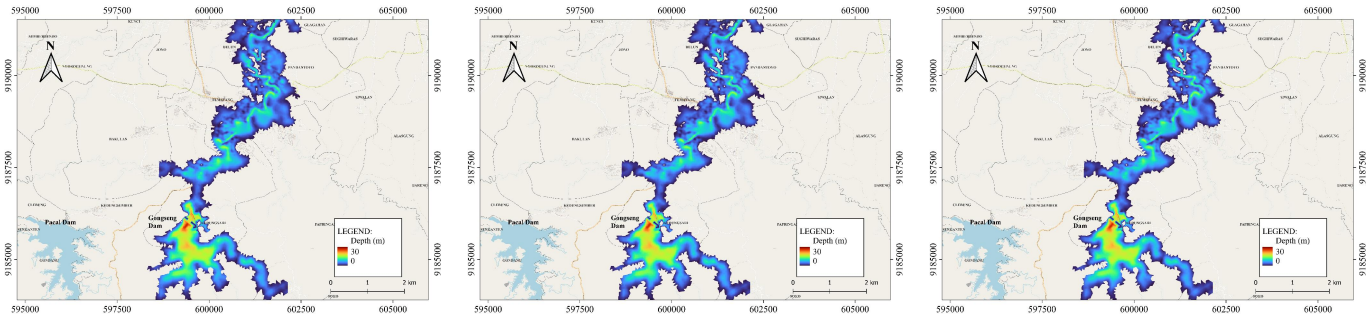

(a) Froehlich (b) Thun (c) USBR

Figure 9 Maps of maximum inundation due to the overtopping scenario

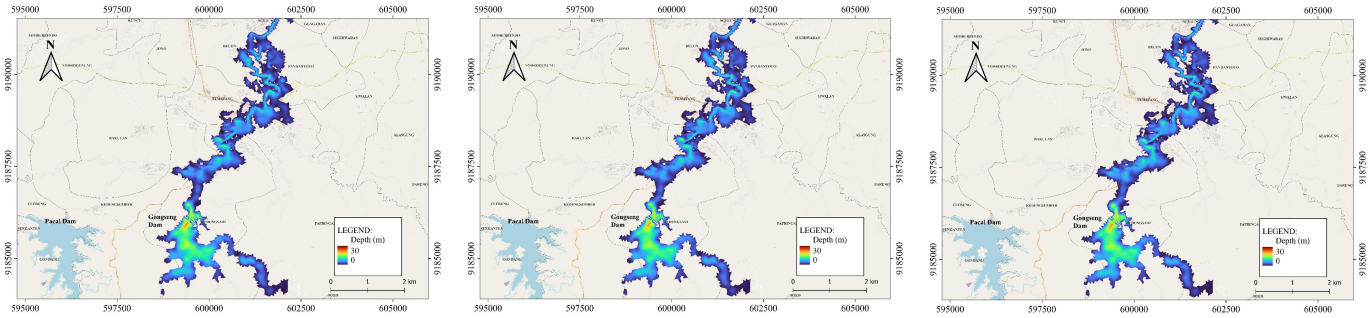

(a) Froehlich (b) Thun (c) USBR

Figure 10 Maps of maximum inundation due to the piping scenario

of 3.12 m s^{-1} and an average speed of 0.84 m s^{-1} were experienced by Papringan as well. Pandantoyo Village, down the stream of Papringan, experienced a maximum velocity to be 1.23 m s^{-1} with average speed of 0.65 m s^{-1}. Belun Village experienced a maximum flood momentum was 0.26 m s^{-1} with average velocity of 0.18 m s^{-1}.

Figure 11 on the right shows the flow velocity based on piping failure mode. The greatest flood velocity that occurred in Kedungsari was 5.21 m s^{-1}, with average velocity of 2.49 m s^{-1}. Kedungsumber Village had a predicted flood velocity of 1.51 m s^{-1} and average speed of 0.96 m s^{-1}. The predicted flood velocity in Temayang was just 0.39 m s^{-1} with average of 0.28 m s^{-1}. Papringan and Pandantoyo had a similar maximum velocity of 0.23 m s^{-1} and average speed of 0.12 m s^{-1}. Similar to the previous sub-section, based on the piping failure mode, Belun Village was not affected by flood.

3.4 Bed Shear Stress

The sediment transport capacity in the riverbed was estimated using various parameters, including critical erosion velocity, bed shear stress, unit crucial discharge, and specific stream power. Bed shear stress remained a frequently used parameter, playing a crucial role in identifying alterations in bed morphology, sedimentation resulting from riverbank erosion, and corrosion connected to river-crossing structures (Petit et al., 2015; Li et al., 2022; Wang et al., 2023). Dam failure simulation results showed that the maximum bed shear stress at Kedung Maor waterfall occurred 0.67 hours after the initiation of dam failure.

Figure 12 shows the evolution of bed shear stress magnitude at Kedung Maor, showcasing variations along various flood discharges. At maximum discharge, the value surged to 1745.42 N m^{-2}, contributing to increased downstream damage.

The erosion resistance of sediment was characterized by critical shear stress. When the flow-induced bed shear stress reached a critical point, sediment movement was ensured, signifying the prediction of initial bed sediment mobilization. Due to the challenges in measuring this stress directly, empirical methods were used for sediment erosion studies (Joshi et al., 2017; He et al., 2021). Iber predicted bed shear stress based on velocity

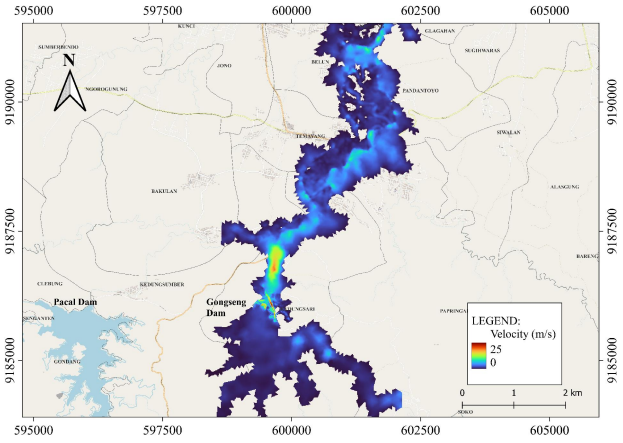

(a) overtopping

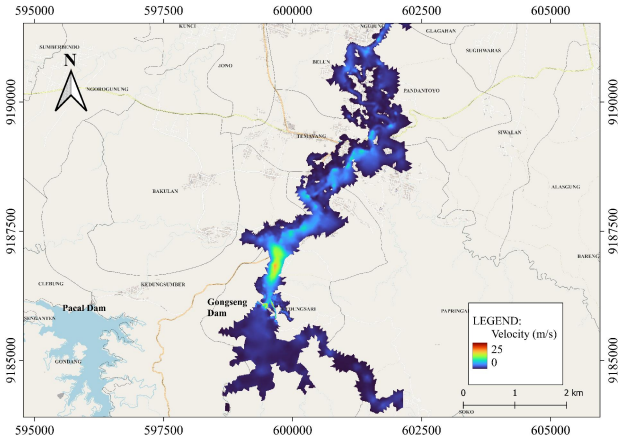

(b) piping failure

Figure 11 Predicted velocity map

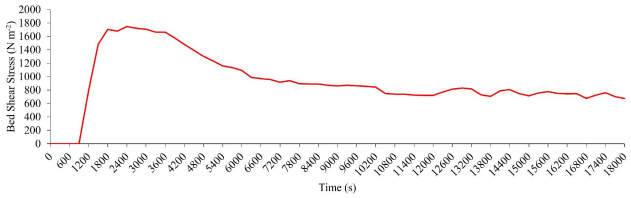

Figure 12 Evolution of bed shear stress at +0.81 km from main dam

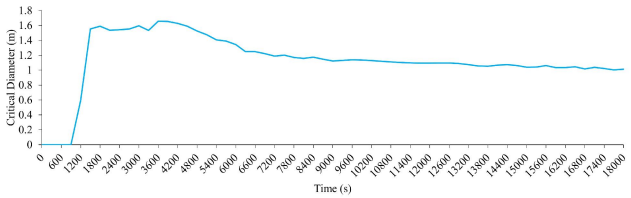

Figure 13 Evolution of critical diameter at +0.81 km from the main dam

at the bottom boundary layer. The magnitude of critical bed shear stress was instrumental in determining the crucial diameter, showing the potential size of sediment particles transportable by flash flood. The efficacy of mathematical modeling in evaluating bed morphology evolution was evident, with a preference for 2D modeling for its simplicity, as shown by Feng et al. (2020); Hu et al. (2020). Figure 13 showed that flood flow was capable of transporting sediment with a relatively large diameter, reaching up to 1.66 m with average diameter of 1.2 m.

Figure 14 shows a bridge located approximately 450 m downstream from the waterfall, connecting Kedungsumber and Kedungsari. Recognizing the potential for severe damage, specific policies and countermeasures were essential to safeguard the

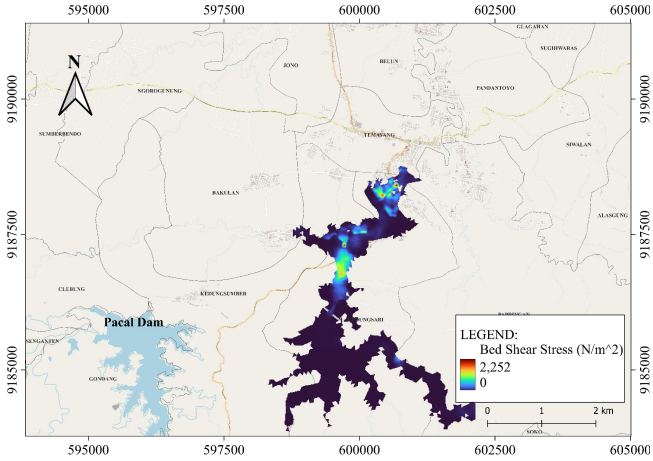

Figure 14 Map of maximum bed shear stress at t = 0.67 hour

bridge.

3.5 Comparison with Real Dam Failure Data

The predicted peak flow was compared with real dam failure data from Pierce et al. (2010). Model results were compared with real-world dam failure to determine the consistency of peak discharge predictions with available observations. Pierce et al. (2010) composite database, which comprised hydrologic and geometric variables from 87 dam break case studies, provided regression relations predicting peak discharge for embankment dam break. Channel resistance expressed as Manning's roughness coefficient 'n', served as the sole parameter required for the hydraulic model calibration. However, flood forecasting applications necessitated data from a similar magnitude flood for calibration, which might not always be available

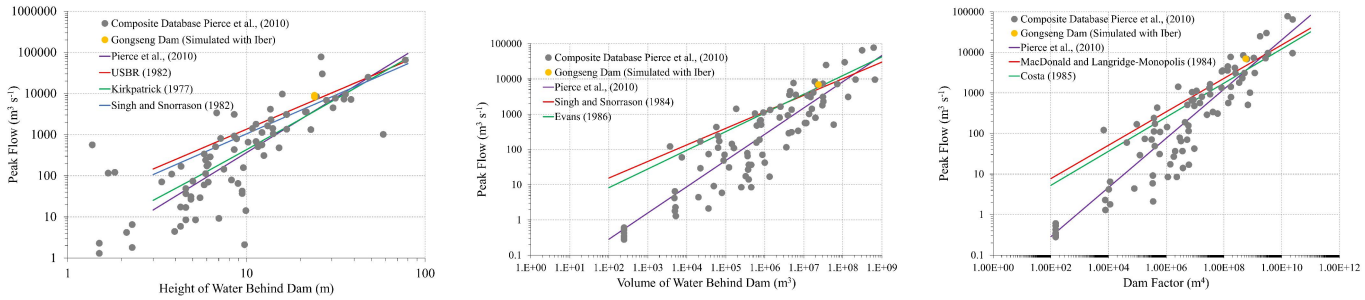

Figure 15 Comparison of the linear best-fit equations of Pierce et al. (2010), U.S. Bureau of Reclamation (1982), Kirkpatrick (1977), Singh and Snorrason (1982), Singh and Snorrason (1984), Evans (1986), MacDonald and Langridge-Monopolis (1984), Costa (1985), and peak flow simulated by Iber model

(Bharath et al., 2021). The Manning's coefficient values also showed spatial variation based on land use, as determined by satellite images, and the selected figures were integrated into Iber model.

Peak flow of 6982.35 m^3 s^{-1} was obtained for Gongseng dam using Evans (1986) equation, with a coefficient of determination R2 of 0.836. This represented approximately a 17% difference in peak discharge from Iber model predictions. Peak discharge predictions correlated with the observations reported by Pierce et al. (2010), as presented in Figure 15, showing the best-fit equation between peak outflow and dam parameters. Iber model predicted peak flow for Gongseng dam correlated reasonably effectively with all historic regression relations.

3.6 Comparison of Empirical Methods

Flood wave propagation occurred in irregular topography, comprising of contractions and expansions due to riverbanks or other obstructions. Although two-dimensional modeling may have simplifications, it still reflected flow conditions, as suggested by Kocaman et al. (2020). The limitations of two-dimensional modeling further led to irrational and excessive values. Users had additional alternatives for adjusting numerical and physical parameter values. The implementation of this approach in dam break analysis yielded acceptable and logical results.

Comparing peak discharge in Figure 16 showed that break geometry significantly impacted flood peak amplitude. Mattas et al. (2023) and this study reiterated the importance of failure time over other characteristics. USBR break volume was

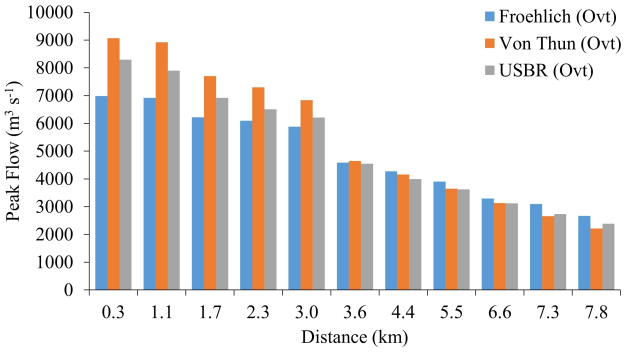

Figure 16 Peak flow due to overtopping for different empirical methods

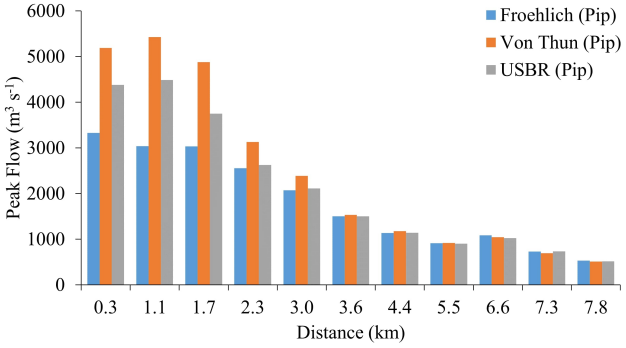

Figure 17 Peak flow due to piping for different empirical methods

smaller than Froehlich, but USBR peak flow was larger, indicating Von Thun method results in the most severe destruction, as observed in Figure 16 Peak discharge values followed the order of Von Thun, USBR, and Froehlich from largest to smallest.

Based on Figure 17, flood propagation downstream decreased to 7.8 km, with Froehlich method resulting in a flatter hydrograph compared to other methods. The flatness was attributed to the time

of failure, with Froehlich bursting resulting in the lowest discharge. Water velocity affected flood inundation and progression downstream, while higher velocity correlated with greater destruction. Additionally, shorter arrival times made evacuation and property protection more challenging. Dam failure was also accompanied by sediment transport, with a greater flow load leading to increased impact force (Mo et al., 2023).

4 CONCLUSION

In conclusion, determining the precise nature of dam failure was a complex undertaking in this study on Gongseng dam. Peak discharge estimates were derived as 6982.35 $m^3 s^{-1}$ (Froehlich), 9070.33 $m^3 s^{-1}$ (Von Thun), and 8296.86 $m^3 s^{-1}$ (USBR). The calculated inundation areas were 7.55 km^2 for piping and 12.57 km^2 for overtopping failures. Overtopping scenarios presented the highest potential discharge, capable of transporting sediment with a significant diameter, reaching up to 1.66 m. The empirical model proposed by Von Thun yielded the most severe damage, particularly impacting Kedungsumber village, where the probable maximum depth of inundation reached 4.58 m and average velocity attained 0.84 m s^{-1}. However, Belun experienced the least impact, with a maximum inundation depth and average velocity of 1.08 m and 0.22 m s^{-1}, respectively. This study considered three various empirical methods for estimating break parameters, with Von Thun method resulting in the most catastrophic consequences, followed by USBR and Froehlich analyses. Von Thun method outperfromed for its capacity to generate the largest break dimensions in a short time, leading to extreme flood events. The Iber model used a 2D technique, assuming velocity averaging over depth, with the potential to limit the accurate understanding of the intensity profiles. Subsequent investigations were promoted to incorporate an advanced turbulence model and higher-resolution DEM to enhance the association of results with real-world conditions. Furthermore, this study recommended the integration of the Pacal Dam into the emergency action plan, reiterating the significance of preparedness in mitigating the potential impact of dam failure.

DISCLAIMER

The authors declare no conflict of interest.

ACKNOWLEDGMENTS

The authors are grateful to the Center for Environmental Studies for the assistance provided and also to Bengawan Solo River Basin Agency for presenting the data required for this study.

REFERENCES

Al-Weshah, R. A., Demissie, M. and Keefer, L. (1993), 'The role of wetlands in stormwater runoff for the Flint and Mutton Creek watersheds, Lake County, Illinois', *ISWS Contract Report CR 562* .

Balai Bendungan, Direktorat Jenderal Sumber Daya Air, Kementrian Pekerjaan Umum dan Perumahan Rakyat (2019), 'Konsep penyusunan rencana tindak darurat'.

Balai Besar Wilayah Sungai Bengawan Solo (2021), 'Database Informasi Sumber Daya Air'.

Bharath, A. et al. (2021), 'Dam break analysis using hec-ras and hec-georas: A case study of Hidkal dam, Karnataka state, India', *Environmental Challenges* **5**, 100401.
URL: *https://doi.org/10.1016/j.envc.2021.100401*

Bladé, E., Cea, L., Corestein, G., Escolano, E., Puertas, J., Vázquez-Cendón, E., Dolz, J. and Coll, A. (2014), *Iber: herramienta de simulación numérica del flujo en ríos*.
URL: *https://doi.org/10.1016/j.rimni.2012.07.004*

Bladé, E. et al. (2014), 'Iber: herramienta de simulación numérica del flujo en ríos', *Revista Internacional de Mètodos Numèricos para Cálculo y Diseño en Ingeniería* **30**(1), 1–10.
URL: *https://doi.org/10.1016/j.rimni.2012.07.004*

Bo, W. et al. (2015), 'A case study of the tangjiashan landslide dam-break', *Journal of Hydrodynamics* **27**(2), 223–233.
URL: *https://doi.org/10.1016/S1001-6058(15)60476-0*

Cea Gómez, L., Bladé i Castellet, E., Sanz-Ramos, M., Bermúdez Pita, M. and Mateos Alonso, Á. (2019), *Iber Applications Basic Guide*, Universidade

da Coruña, Servizo de Publicacións, A Coruña.
URL: *https://doi.org/10.17979/spudc.9788497497176*

Cea, L. and Bladé, E. (2015), 'A simple and efficient unstructured finite volume scheme for solving the shallow water equations in overland flow applications', *Water Resources Research* **51**, 5464–5486.
URL: *https://doi.org/10.1002/2014WR016547*

Cea, L., Garrido, M. and Puertas, J. (2010), 'Experimental validation of two-dimensional depth-averaged models for forecasting rainfall – runoff from precipitation data in urban areas', *Journal of Hydrology* **382**(1–4), 88–102.
URL: *https://doi.org/10.1016/j.jhydrol.2009.12.020*

Cea, L., Puertas, J. and Vázquez-Cendón, M.-E. (2007), 'Depth averaged modelling of turbulent shallow water flow with wet-dry fronts', *Arch Comput Methods Eng.* pp. 303–341.
URL: *https://doi.org/10.1007/s11831-007-9009-3*

Costa, J. E. (1985), Floods from dam failures, Open-File Rep. 85-560, U. S. Geological Survey, Denver, Colorado.

da Hora, M. d. A. G., de Miranda Neto, M. I. et al. (2018), 'Classification of the Juturnaíba Dam: Potential risk and damage', *Journal of Water Resource and Protection* pp. 1–19.
URL: *https://doi.org/10.4236/jwarp.2018.101001*

Evans, S. G. (1986), 'The maximum discharge of outburst floods caused by the breaching of man-made and natural dams', *Can. Geotech. J.* **23**(3), 385–387.
URL: *https://doi.org/10.1139/t86-053*

Feng, Z. et al. (2020), 'Two-dimensional numerical simulation of sediment transport using improved critical shear stress methods', *International Journal of Sediment Research* **35**(1), 15–26.
URL: *https://doi.org/10.1016/j.ijsrc.2019.10.003*

Froehlich, D. C. (2008), 'Embankment dam breach parameters and their uncertainties', *Journal Hydraullic Engineering* **134**, 1708–1721.
URL: *https://doi.org/10.1061/(ASCE)0733-9429(2008)134:12(1708)*

Guo, L. et al. (2022), 'Water demand forecasting and countermeasures across the yellow river basin: Analysis from the perspective of water resources carrying capacity', *Journal of Hydrology: Regional Studies* **42**, 101148.
URL: *https://doi.org/10.1016/j.ejrh.2022.101148*

He, C. et al. (2021), 'A new portable in situ flume for measuring critical shear stress on river beds', *International Journal of Sediment Research* **36**(2), 235–242.
URL: *https://doi.org/10.1016/j.ijsrc.2020.08.004*

Hu, P., Xie, J., Li, W., He, Z., Marsooli, R. and Wu, W. (2020), 'A rans numerical study of experimental swash flows and its bed shear stress estimation', *Applied Ocean Research* **100**, 102145.
URL: *https://doi.org/10.1016/j.apor.2020.102145*

Jia, Y. and Wang, S. S. Y. (1999), 'Numerical model for channel flow and morphological change studies', *Journal Hydraulic Engineering* pp. 924–933.
URL: *https://doi.org/10.1061/(ASCE)0733-9429(1999)125:9(924)*

Joshi, S., Patrick, G. and Brown, C. (2017), 'Critical bed shear stress and threshold of motion of maerl biogenic gravel', *Estuarine, Coastal, and Shelf Science* **194**, 128–142.
URL: *https://doi.org/10.1016/j.ecss.2017.06.010*

Kao, H. and Chang, T. (2012), 'Numerical modeling of dam-break-induced flood and inundation using smoothed particle hydrodynamics', *Journal of Hydrology* **448–449**, 232–244.
URL: *https://doi.org/10.1016/j.jhydrol.2012.05.004*

Khosravi, K., Rostaminejad, M., Cooper, J. R., Mao, L. and Melesse, A. M. (2016), Dam break analysis and flood inundation mapping: The case study of Sefid-Roud Dam, Iran, *in* 'Extreme Hydrology and Climate Variability', Elsevier Inc.
URL: *https://doi.org/10.1016/B978-0-12-815998-9.00031-2*

Kirkpatrick, G. W. (1977), Evaluation guidelines for spillway adequacy, *in* 'Proc., Engineering Foundation Conf.', ASCE, Reston, Va., pp. 395–414.

Kocaman, S. et al. (2020), 'Experimental and numerical analysis of a dam-break flow through different contraction geometries of the channel', *Water* **12**, 1–22.
URL: *https://doi.org/10.3390/w12041124*

Li, M. et al. (2022), 'Effects of antecedent soil moisture on rill erodibility and critical shear stress', *Catena* **216(PA)**, 106356.
URL: *https://doi.org/10.1016/j.catena.2022.106356*

MacDonald, T. C. and Langridge-Monopolis, J. (1984), 'Breaching characteristics of dam failures', *J. Hydraul. Eng.* **110**(5), 567–586.
URL: *https://doi.org/10.1061/(ASCE)0733-9429(1984)110:5(567)*

Mattas, C. et al. (2023), 'Two-dimensional modelling for dam break analysis and flood hazard mapping: A case study of papadia dam, northern greece', *Water* **15**, 1–25.
URL: *https://doi.org/10.3390/w15050994*

Mo, C. et al. (2023), 'Simulation of one-dimensional dam-break flood routing based on hec-ras', *Frontiers in Earth Science* pp. 1–15.
URL: *https://doi.org/10.3389/feart.2022.1027788*

Oliveira, A. M. et al. (2022), 'Loss of life estimation and risk level classification due to a dam break', *Heliyon* **8**, 1–12.
URL: *https://doi.org/10.1016/j.heliyon.2022.e09257*

Petit, F. et al. (2015), 'Dimensionless critical shear stress in gravel-bed rivers', *Geomorphology* **250**, 308–320.
URL: *https://doi.org/10.1016/j.geomorph.2015.09.008*

Pierce, M. et al. (2010), 'Predicting peak outflow from breached embankment dams', *Journal of Hydraulic Eng.* pp. 338–349.
URL: *https://doi.org/10.1061/(ASCE)HE.1943-5584.0000197*

Singh, K. P. and Snorrason, A. (1982), Sensitivity of outflow peaks and flood stages to the selection of dam breach parameters and simulation models, Contract Rep. 288, State Water Survey (SWS).
URL: *https://doi.org/10.1016/0022-1694(84)90217-8*

Singh, K. P. and Snorrason, A. (1984), 'Sensitivity of outflow peaks and flood stages to the selection of dam breach parameters and simulation models', *J. Hydrol.* **68**, 295–310.
URL: *https://doi.org/10.1016/0022-1694(84)90217-8*

U.S. Bureau of Reclamation (1982), Guidelines for defining inundated areas downstream from bureau of reclamation dams, Reclamation Planning Instruction Rep. 82-11.

Wahl, T. L. (2004), 'Uncertainty of predictions of embankment dam breach parameters', *Journal of Hydraulic Engineering* pp. 389–397.
URL: *https://doi.org/10.1061/(ASCE)0733-9429(2004)130:5(389)*

Wang, X., Gualtieri, C. and Huai, W. (2023), 'Grain shear stress and bed-load transport in open channel flow with emergent vegetation', *Journal of Hydrology* **618**(February), 129–204.
URL: *https://doi.org/10.1016/j.jhydrol.2023.129204*

Wu, W. (2004), 'Depth-averaged two-dimensional numerical modeling of unsteady flow and nonuniform sediment transport in open channels', pp. 1013–1024.
URL: *https://doi.org/10.1061/(ASCE)0733-9429(2004)130:10(1013)*

Álvarez, M. et al. (2017), 'Two-dimensional dam-break flood analysis in data-scarce regions: The case study of Chipembe Dam, Mozambique', *Journal of Water* pp. 1–19.
URL: *https://doi.org/10.3390/w9060432*

[This page is intentionally left blank]